# A Study on the Behavior Characteristics of Diesel Spray by Using a High Pressure Injection System with Common Rail Apparatus

**Jeong-Kuk Yeom***
*Department of Automotive Engineering, Silla University, San 1-1, Gwaebop-dong, Sasang-gu, Pusan 617-736, Korea*
**Hajime Fujimoto**
*Department of Mechanical Engineering, Doshisha University, Kyotanabe, Kyoto, Japan*

The effects of change in injection pressure on spray structure in high temperature and pressure field have been investigated. The analysis of liquid and vapor phases of injected fuel is important for emissions control of diesel engines. Therefore, this work examines the evaporating spray structure using a constant volume vessel. The injection pressure is selected as the experimental parameter, is changed from 22 MPa to 112 MPa using a high pressure injection system (ECD-U2). Also, we conducted simulation study by modified KIVA-II code. The results of simulation study are compared with experimental results. The images of liquid and vapor phase for free spray were simultaneously taken by exciplex fluorescence method. As experimental results, the vapor concentration of injected fuel is leaner due to the increase of atomization in the case of the high injection pressure than in that of the low injection pressure. The calculated results obtained by modified KIVA-II code show good agreements with experimental results.

**Key Words :** Spray Structure, Emission Control, KIVA-II Code, Exciplex Fluorescence Method, Spray Simulation

## 1. Introduction

In diesel engines, atomization, evaporation, and mixture formation process of injected liquid fuel affect ignition characteristics and combustion process. However, the process and structure of injected spray have not been cleared yet due to the unsteady flow processes which are induced by high pressure fuel injection, breakup, atomization, and turbulent entrainment process of ambient gas. The papers about development mechanism of diesel spray have been reported by Wakuri et al.(1959), Hiroyasu et al.(1980), and Dan et al.(1997). However, the previous studies had been conducted in non-evaporating diesel spray (Wakuri et al., 1959 ; Hiroyasu et al., 1980) and experimental results of Dan et al.(1997) had been obtained from condition of lower injection pressure. Therefore, this study examines the evaporating spray structure using a constant volume vessel in high temperature and pressure field. On the other hand, we conducted simulation study by modified KIVA-II code (Amsden, et al., 1985, 1989, 1993, 1997) proposed by the Los Alamos Lab. The $\Phi$ and $K$ of the improved TAB model used in this study are, respectively, 6 and 0.89, as in the non-evaporating spray (Senda et al., 1997).

* Corresponding Author,
**E-mail** : laser355@hanmail.net
**TEL** : +82-51-200-6714; **FAX** : +82-51-200-7656
Department of Automotive Engineering, Silla University, San 1-1, Gwaebop-dong, Sasang-gu, Pusan 617-736, Korea. (Manuscript **Received** December 26, 2002; **Revised** June 2, 2003)

## 2. Experimental Apparatus and Procedure

Figure 1 is a schematic diagram of experimental apparatus. The constant volume vessel has two quartz glass windows ($\Phi$=120 mm×45 mm

width) permitting the spray inside to be irradiated with a sheet of laser light and allowing the fluorescence emissions from the spray to be measured. Each of the windows was perpendicularly installed. The n-tridecane, as the reference fuel oil of JIS second class gas oil, was injected into the quiescent atmosphere of nitrogen gas through an injector with single hole. 9% in mass of naphthalene and 1% in that of TMPD (N, N, N', N' tetramethyl-p-phenylene diamine) were mixed in n-tridecane to obtain the fluorescent emissions of vapor and liquid phases. The high pressure injection system (ECD-U2 system) was proposed by Denso Co., Ltd.. This system consists of three main sections, namely, high pressure supply pump, common rail and control circuit (ECU), which controls the injector. The diameter and the length of nozzle were respectively 0.2 mm and 1.0 mm. The injection pressure was changed in the range from 22 MPa to 112 MPa. The injection duration was varied in the range from 2.82 msec. to 1.24 msec., and the quantity of the injected fuel was constantly kept as 12.0 mg. The detailed explanation about the experimental apparatus and optical system is also found in Yeom et al. (2002). Table 1 shows the experimental conditions of this study.

**Table 1** Experimental conditions

| | | |
|---|---|---|
| Injection nozzle | Type: Hole nozzle DLL-p | |
| | Diameter of hole $d_n$ [mm] | 0.2 |
| | Length of hole $L_n$ [mm] | 1.0 |
| Ambient gas | | $N_2$ gas |
| Ambient temperature $T_a$ [K] | | 700 |
| Ambient pressure | $p_a$ [MPa] | 2.55 |
| Ambient density | $\rho_a$ [kg/m$^3$] | 12.3 |
| Injection pressure | $p_{inj}$ [MPa] | 22, 42, 72, 112 |
| Injection quantity | $Q_{inj}$ [mg] | 12.0 |
| Injection duration | $t_{inj}$ [ms] | 2.82, 1.98, 1.54, 1.24 |

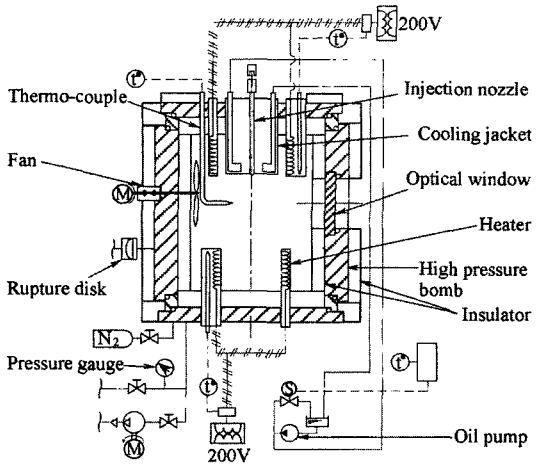


**Fig. 1** Experimental apparatus

## 3. Review on KIVA-II Code with the TAB Model

The results calculated by KIVA-II code with the TAB model were compared with the experimental results. The profiles of the size distribution changed, i.e. the degree of freedom $\Phi$ of the $\chi$-squared function. The distorting motion of particles was discussed in terms of its energy ratio, i.e. the parameter $K$ of the TAB method. This study, like the non-evaporating spray (Senda et al., 1997), tunes the parameters $\Phi$ and $K$ for each case of $\Phi=2$, $K=10/3$ and $\Phi=6$, $K=0.89$, respectively. In each case, the distribution function $f(r)$, the weight distribution function $g(r)$ and the cumulative distribution function $h(r)$ are expressed by the following equations.

[Case of $\Phi=2$]

$$f(r)=\frac{1}{\bar{r}}\exp\left[-\frac{r}{\bar{r}}\right] \tag{1}$$

$$g(r)=\frac{r^3}{6\bar{r}^4}\exp\left[-\frac{r}{\bar{r}}\right] \tag{2}$$

$$h(r)=\int_0^r g(r)\,dr$$
$$=1-\left[1+\frac{r}{\bar{r}}+\frac{1}{2}\left(\frac{r}{\bar{r}}\right)^2+\frac{1}{6}\left(\frac{r}{\bar{r}}\right)^3\right]\times\exp\left[-\frac{r}{\bar{r}}\right], \tag{3}$$
$$r\le\frac{r}{\bar{r}}\le 12$$

[Case of $\Phi=6$]

$$f(r)=\frac{r^2}{6\bar{r}^3}\exp\left[-\frac{r}{\bar{r}}\right] \tag{4}$$

$$g(r)=\frac{r^5}{120\bar{r}^6}\exp\left[-\frac{r}{\bar{r}}\right] \tag{5}$$

$$h(r)=\int_0^r g(r)\,dr$$
$$=1-\left[1+\frac{r}{\bar{r}}+\frac{1}{2}\left(\frac{r}{\bar{r}}\right)^2+\frac{1}{6}\left(\frac{r}{\bar{r}}\right)^3+\frac{1}{24}\left(\frac{r}{\bar{r}}\right)^4+\frac{1}{120}\left(\frac{r}{\bar{r}}\right)^5\right]\times\exp\left[-\frac{r}{\bar{r}}\right],\quad r\le\frac{r}{\bar{r}}\le 21 \tag{6}$$

Where $r$ is the particle radius and $\bar{r}$ is the arithmetic average radius of the particles. For each distribution function $f(r)$, $\bar{r}$ is related to the input Sauter mean radius $r_{32}$, $\bar{r}=r_{32}/3$ [for Eq. (1)] and $\bar{r}=3r_{32}/5$ [for Eq. (4)]. In the TAB method (O'rourke et al., 1987), the motion of a particle is described with conservation of its energy before breakup $E_{old}$ and after breakup $E_{new}$. The equations for $E_{old}$ and $E_{new}$ are given by the following.

$$E_{old}=4\pi r^2\sigma+K\frac{\pi}{5}\rho_d r^5(\dot{y}+\omega'^2y^2) \tag{7}$$

$$E_{new}=4\pi r^2\sigma\frac{r}{r_{32}}+\frac{\pi}{6}\rho_d r^5\dot{y} \tag{8}$$

Where, $r$ is the particle radius before breakup and $r_{32}$ is the Sauter mean radius after breakup, and $\sigma$ is the surface tension of particle, and $\rho_d$ is particle density, and $y$ is the non-dimensional displacement of the particle surface and $\omega'$ is the oscillation frequency. $K$ is the ratio of the distorting energy of particle to its total energy. Assuming conservation of energy in particle motion with $y=1$ in oscillation and breakup, the following equation can be obtained from setting Eq. (7)=Eq. (8).

$$r_{32}=\frac{r}{\left[1+\frac{8K}{20}+\frac{6K-5}{120}\left(\frac{\rho_d r^3}{\sigma}\right)\dot{y}^2\right]} \tag{9}$$

The energy ratio $K$ is determined as $K=10/3$ in the original TAB model (O'rourke et al., 1987).

Figure 2 shows the spray tip penetration versus time for the various $\Phi$ and $K$. As shown this figure, it can be concluded that the cases of $\Phi=6$ and $K=0.89$ could successfully estimate the actual droplets distribution and spray tip penetration in the diesel spray.

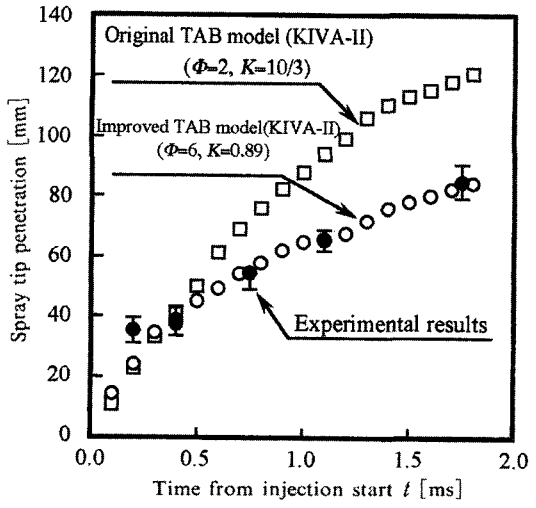


**Fig. 2** Temporal change in spray tip penetration for calculational and experimental results ($Q_{inj}$=12.0 [mg], $p_{inj}$=72 [MPa], $\rho_a$=12.3 [kg/m$^3$], $T_a$=700 [K])

## 4. Results and Discussion

### 4.1 Experiment results

Figure 3 shows the two-dimensional fluorescence intensity images of the free spray with injection pressure change obtained by exciplex fluorescence method. In the images, (i), (ii) are the vapor and liquid phase of the injected fuel, respectively. The photographing timing, $t$ was set when the injected fuel mass was almost the same in the each injection pressure, that is, when $t/t_{inj}$ was almost equal at each injection pressure. In the each figure, the liquid phase is wider than the vapor phase in the upper region of the spray, because photographing the vapor phase, a aperture of large value was selected in order to reduce the halation region due to the strong TMPD monomer fluorescence of liquid phase. On the other hand, when photographing the liquid phase, the aperture of small value was selected in the optical system to capture the liquid phase region of low concentration. Consequently, the liquid phase image is larger than the vapor phase image. In the Fig. 3, the low vapor luminance of the upstream spray spreads in the radial direction. With increasing injection pressure, the atomization and evaporation of the diesel spray were promoted by the increase of shear force caused by the interaction between the injected fuel and ambient

gas. The fluorescence intensity of the liquid phase rapidly decreases in the vicinity of $Z=40$ mm from the nozzle tip. Also, in each condition of injection pressure, the meandering flow of the mainstream region starts on the spray radial direction at the distance of $Z=40$ mm. It could be speculated that the transition point at which the momentum of the spray interchanges with the ambient gas is, approximately, in the vicinity of $Z=40$ mm. Consequently, the vortex flow of the ambient gas dominates spray development in the latter part of the injection.

Figure 4 shows the temporal change in spray tip penetration of the vapor and liquid phase. In

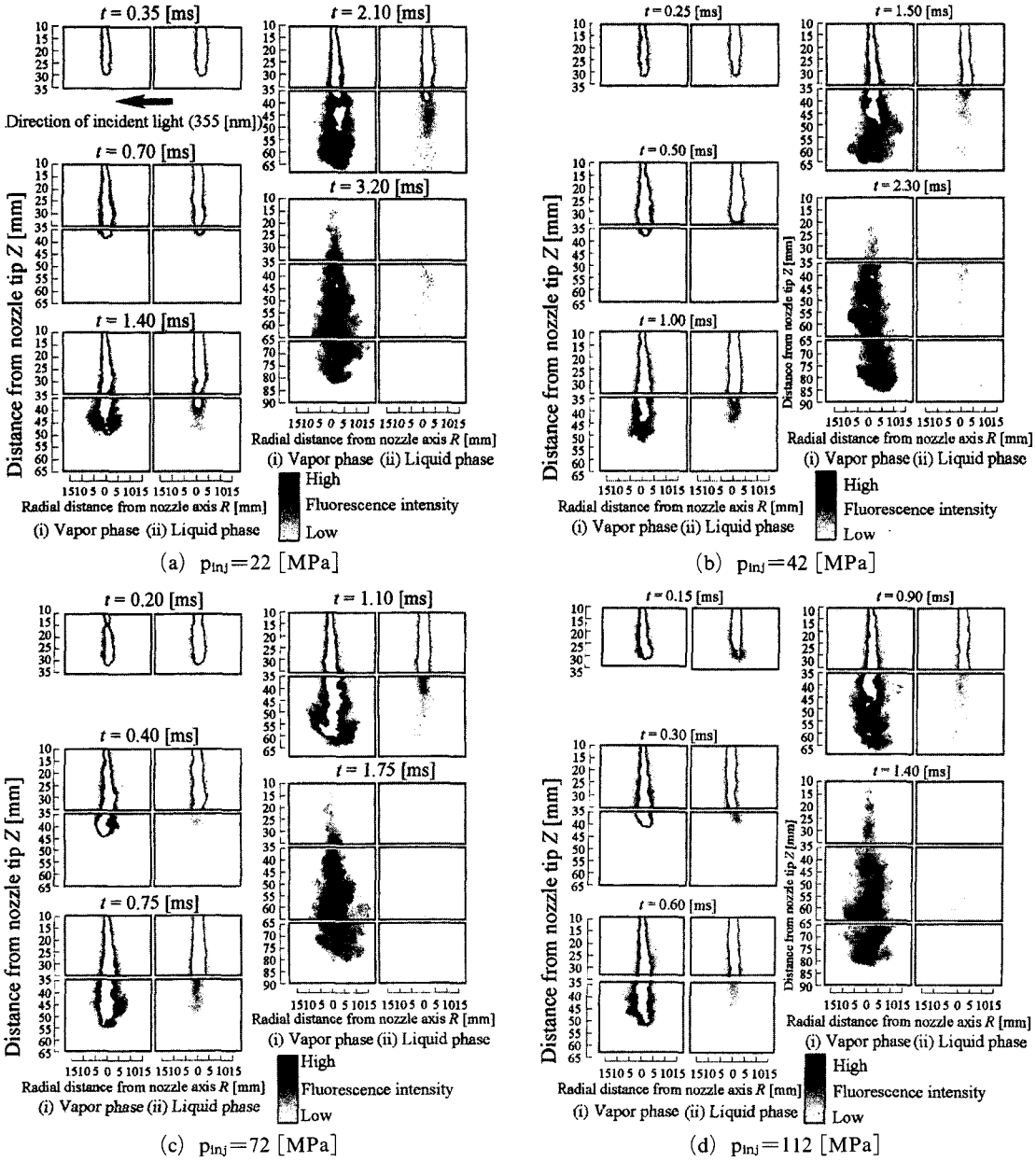


**Fig. 3** Temporal change in spray image with exciplex fluorescence method ($Q_{inj}=12.0$[mg], $\rho_a=12.3$[kg/m$^3$], $T_a=700$[K])

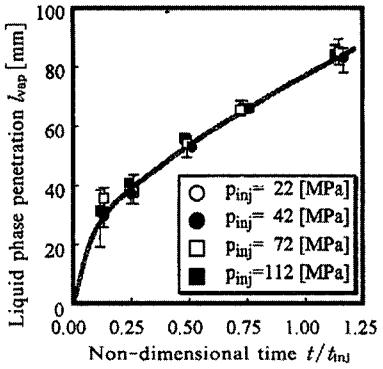


(a) Vapor phase pentration $l_{vap}$

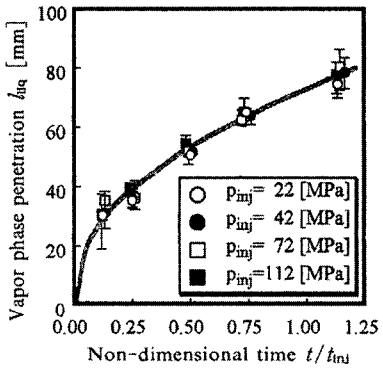


(b) Liquid phase penetration $l_{liq}$

**Fig. 4** Temporal change in penetration of vapor and liquid phase (Parameter : Injection pressure)

the figure, the horizontal axis is the non-dimensional time from the start of injection with each injection duration. The spray tip penetration of liquid phase $l_{liq}$ is determined by the overall fluorescence intensity region in the images. Then, the penetrations at each injection pressure is compared with the same mass of injected fuel, because the profile of the injection rate with time is almost rectangular in this study. The spray tip penetrations of the vapor and the liquid phase were plotted in the same curve as shown in Fig. 4. Consequently, they are independent of injection pressure in non-dimensional time. As a result, the spray tip penetration when the same mass of fuel is injected does not depend on injection pressure. The same result was observed in non-evaporating diesel spray (Dan et al., 1996a). As shown in Fig. 4, the penetration of liquid and vapor phase increase with elapsing time. However, a convergence tendency of the liquid phase length, as

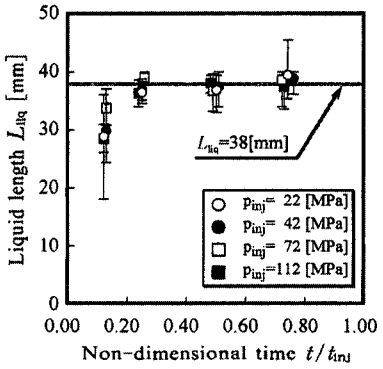


**Fig. 5** Temporal change in liquid length (Parameter : Injection pressure)

shown in the other experiments using evaporating spray (Hodges et al., 1991 ; Baritaud et al., 1994 ; Espey et al., 1997), could not be observed.

Figure 5 shows the liquid length $L_{liq}$ versus the elapsing non-dimensional time. In this study, the liquid length $L_{liq}$ is defined by the spatial region where the maximum value (255 gradation) of fluorescence intensity decreases to 10% (230 gradation) at central axis of liquid phase images. As shown in Fig. 5, the value of the liquid length is almost 38 mm in the curve. As a result, the liquid length as measured in Fig. 5 is equal to the liquid phase lengths of the experiments by Hodges et al., 1991 ; Baritaud et al., 1994 ; Espey et al., 1997. Moreover, the behavior tendency of liquid phase was found to change at the start point of spray development in the radial direction as shown in Fig. 3. This means that the distance of 38 mm from nozzle exit corresponds to the end of momentum exchange from the liquid jet to the ambient gas in non-evaporating spray (Dan et al., 1996a).

### 4.2 Calculation results

Figure 6 shows the calculation results with the improved TAB model. In this figure, (a) shows droplet parcels, (b) shows vapor concentration of injected fuel, (c) shows droplet velocity, and (d) shows spatial distribution of ambient gas velocity. In calculation results of Figs. 6-(b), vapor phase flock formed in the images of experimental results by improved atomization due to the shear-force both injected fuel and ambient gas near the nozzle

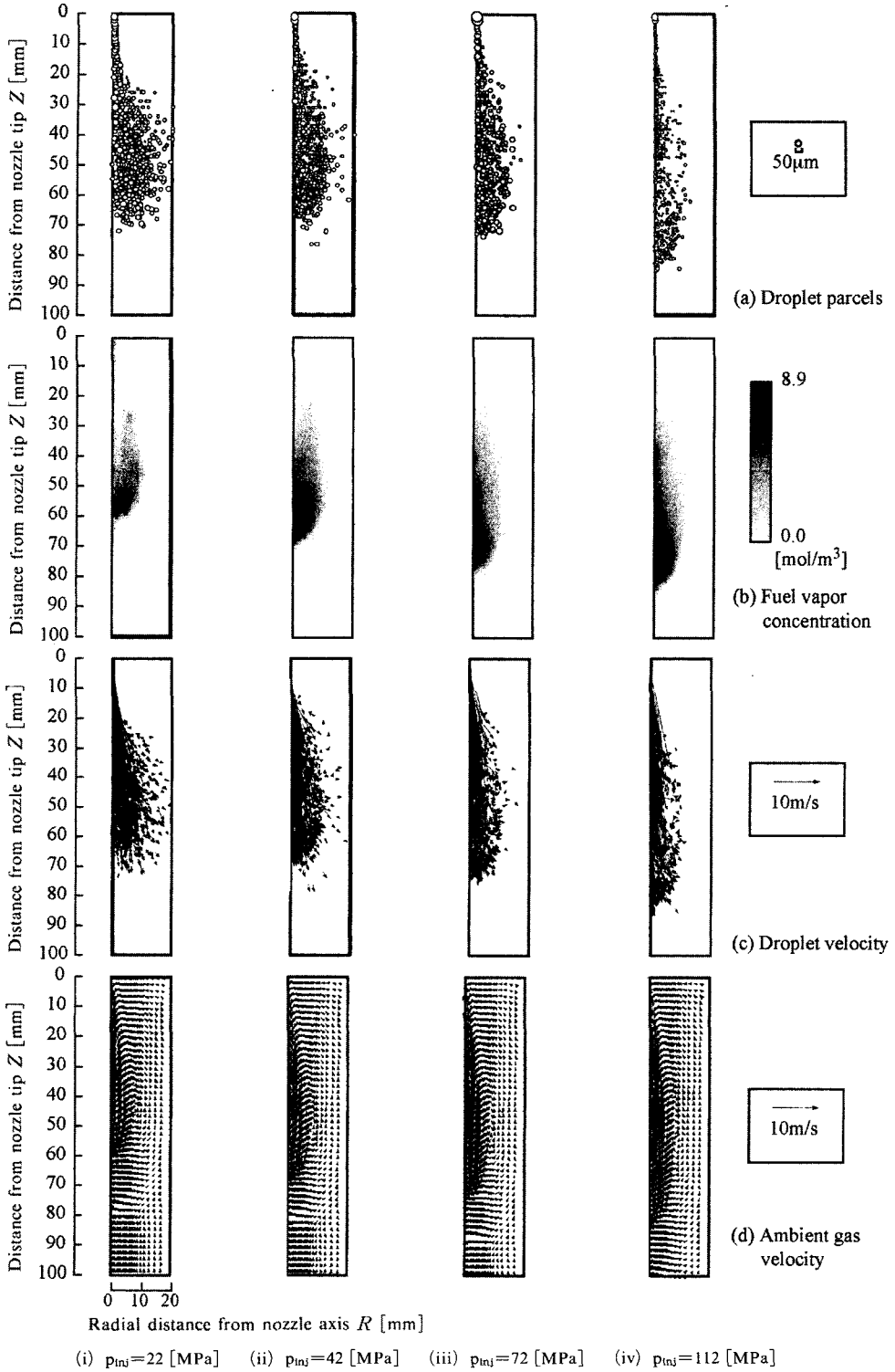


**Fig. 6** Temporal change in spatial distribution of droplet parcels, fuel vapor concentration, droplet velocity, and ambient gas velocity with improved KIVA-II code at $t=1.50$ [ms] from injection start ($t_{inj}=1.54$ [ms], $\rho_a=12.3$ [kg/m$^3$] ; Parameter : Injection pressure)

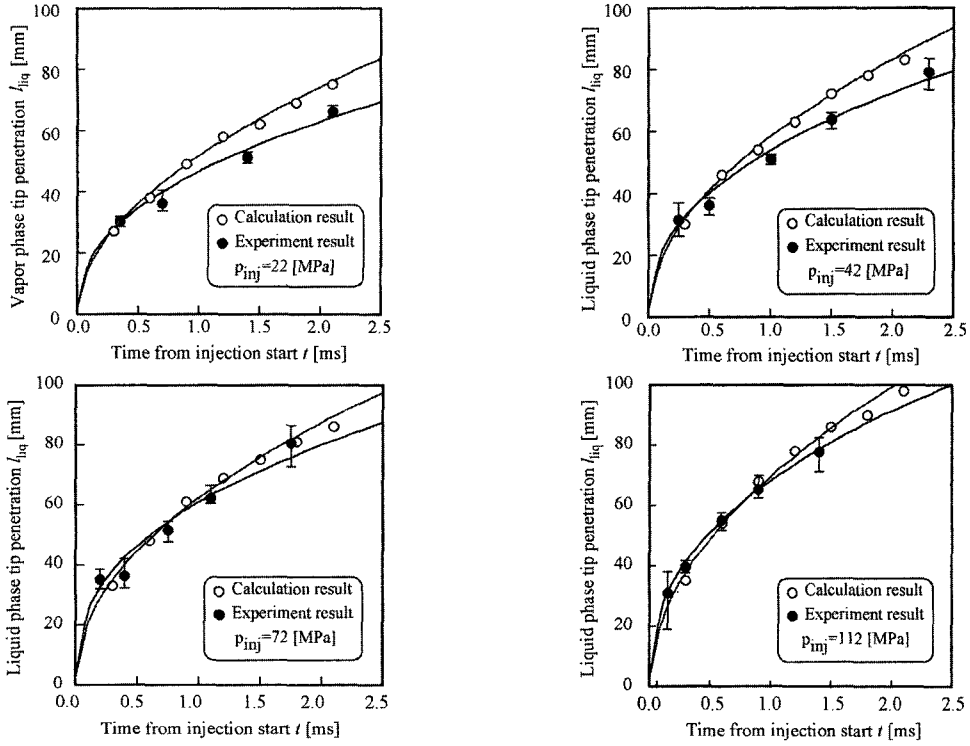


(a) Liquid phase

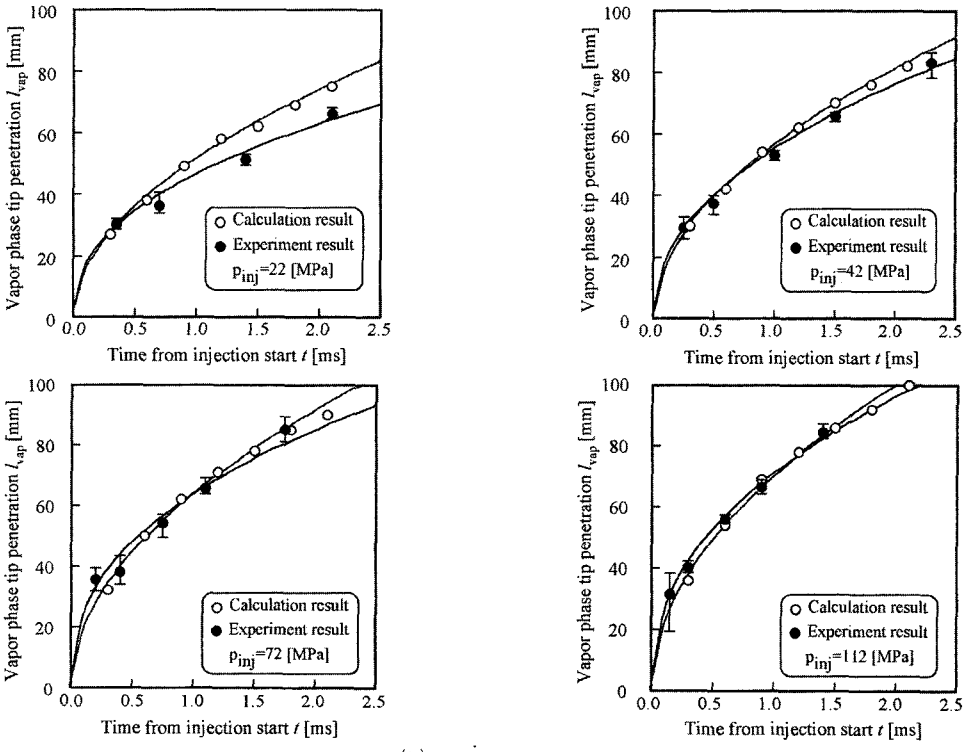


(b) Vapor phase

**Fig. 7** Temporal change in penetration of vapor and liquid phase ($Q_{inj}$=12 [mg], $\rho_a$=12.3 [kg/m$^3$])

could not be investigated. The reason is that the KIVA-II code for the calculation of droplet breakup uses the TAB breakup model which is based on oscillation and distortion of droplets. Thus, there is no atomized droplets and the formation of vapor phase caused by shear-force in the vicinity of nozzle, and the droplets become larger near the nozzle. Furthermore, as for a remarkable difference between the calculation results and the experimental results, it can be found that the distribution of droplet parcels widely spreads in the radial direction and the high concentration region of fuel vapor concentrates on the region of the spray tip due to the underestimation for the amount of droplet evaporation. It is necessary to modify the droplet evaporation model by comparing the experimental results of spray development process. Figure 6-(c) shows velocity distribution of droplets. The velocity vectors of droplets near the center of spray are developing along the axis of the spray. On the other hand, the velocity distribution of the droplets is irregular tendency at the region of spray periphery, because the droplets which lose the momentum obey to ambient gas flow. As shown in Fig. 6-(d), the ambient gas is entrained into the spray and is proceeding along the central axis of the spray. Moreover, the entrained ambient gas revolves in the radial direction, and there is the vertical velocity component of the entrained ambient gas in the spray periphery. This spray structure is different from the reported experiment results (Dan et al., 1996b) which show the vortex structure distribution of larger scale with proceeding in downstream of the spray. However, the spray formation mechanism, like experimental results can be also speculated from the results of KIVA-II code, namely, the motion of ambient gas is induced by the fuel injection, and the vortex flow induced by droplets and vapor fuel dominates spray spreading.

Figure 7 shows the temporal change in tip penetration of liquid and vapor fuel. In the Fig. 7, the results from modified TAB model is a good agreement with experimental results, and the modified KIVA-II code can successfully reproduce the diesel spray behavior in evaporating field.

## 5. Conclusions

The following conclusions are drawn from this study.

(1) The penetration of evaporating diesel spray when the same mass of fuel is injected does not depend on injection pressure in non-dimensional time.

(2) With increasing injection pressure, the atomization and evaporation of the diesel spray are promoted by the increase of shear force caused by the interaction between the injected fuel and ambient gas.

(3) Applying the modified TAB model of $\Phi$ (degree of freedom) $=6$ and $K$ (energy ratio of particle motion) $=0.89$ to evaporating fuel spray is sufficiently useful for analyzing macro structure of the spray, such as spray tip penetration of liquid and vapor phase.

## References

Amsden, A. A., Ramshow, J. D., O'Rourke, P. J. and Dukowiez, J. K., 1985, "KIVA : A Computer Program for Two- and Three-Dimensional Fluid Flows with Chemical Reactions and Fuel Sprays," *Los Alamos National Laboratory Report* LA-10254-MS.

Amsden, A. A., O'Rourke, P. J. and Butler, T. D., 1989, "KIVA-II : A Computer Program for Chemically Reactive Flows and Sprays," *Los Alamos National Laboratory Report* LA-11560-MS.

Amsden, A. A., 1993, "KIVA-3 : A KIVA Program with Block-Structured Mesh for Complex Geometries," *Los Alamos National Laboratory Report* LA-12503-MS.

Amsden, A. A., 1997, "KIVA-3V : A Block-Structured KIVA Program for Engines with Vertical or Canted Valves," *Los Alamos National Laboratory Report* LA-13313-MS.

Baritaud, T. A., Heinze, T. A. and Le Coz, J. F., 1994, "Spray and Self-Ignition Visualization in a D.I. Diesel Engine," *SAE Paper*, No. 940681.

Dan, T., Takagishi, S., Senda, J. and Fujimoto, H., 1997, "Organized Structure and Motion in

Diesel Spray," *SAE Paper*, No. 970641.

Dan, T., Takagishi, S., Oishi N., Senda J. and Fujimoto, H., 1996a, "The Study of the Spray Structure in the High Injection Pressre," *JSME* 62-597, pp. 2079~2085, (in Japanese).

Dan, T., Takagishi, S., Oishi N., Senda J. and Fujimoto, H., 1996b, "The Effect of Ambient Density on the Spray Structure," *JSME* 62-599. pp. 2867~2083, (in Japanese).

Espey, C., Dec, J. E., Litzinger, T. A. and Santavicca, D. A., 1997, "Planar Laser Rayleigh Scattering for Quantitative Vapor-Fuel Imaging in a Diesel Jet," COMBUSTION AND FLAME, 109 : 65-86, pp. 65~86.

Hiroyasu, H. and Arai, M., 1980, "Fuel Spray Penetration and Spray Angle in Diesel Engines," *JSAE*, No. 21, pp. 5~11, (in Japanese).

Hodges, J. T., Baritaud, T. A. and Heinze, T. A., 1991, "Planar Liquid and Gas Fuel and Droplet Size Visualization in a DI Diesel Engine," *SAE Paper*, No. 910726.

O'Rourke, P. J. and Amsden, A. A., 1987, "The TAB Method for Numerical Calculation of Spray Drop Breakup," *SAE Paper*, No. 872089.

Senda, J., Kanda, T., Al-Roub, M., Farrell, P. V., Fukami, T. and Fujimoto, H., 1997, "Modeling Spray Impingement Considering Fuel Film Formation on the Wall," *SAE Paper*, No. 970047.

Wakuri, Y., Fujii M., Amitani, T. and Tsuneya R., 1959, "Studies on the Penetration of Fuel Spray of Diesel Engine," *JSME* (part2), Vol. 52, No. 156, pp. 820~826, (in Japanese).

Yeom, J. K., Kang, B. M., Lee, M. J., Chung, S. S., Ha, J. Y. and Fujimoto, H., 2002, "A Study on the Mixture Formation Process of Evaporating Diesel Spray by Offset Incidence Laser Beam," *KSME International Journal*, Vol. 16, No. 12, pp. 1702~1709.